



HAL
open science

Axisymmetric wave propagation in multilayered poroelastic grounds due to a transient acoustic point source

Julien Capeillère, Arnaud Mesgouez, Gaëlle Lefeuvre-Mesgouez

► **To cite this version:**

Julien Capeillère, Arnaud Mesgouez, Gaëlle Lefeuvre-Mesgouez. Axisymmetric wave propagation in multilayered poroelastic grounds due to a transient acoustic point source. *Soil Dynamics and Earthquake Engineering*, 2013, 52 (September 2013), pp.70-76. 10.1016/j.soildyn.2013.05.003. hal-00734083v5

HAL Id: hal-00734083

<https://hal.science/hal-00734083v5>

Submitted on 2 Jul 2013

HAL is a multi-disciplinary open access archive for the deposit and dissemination of scientific research documents, whether they are published or not. The documents may come from teaching and research institutions in France or abroad, or from public or private research centers.

L'archive ouverte pluridisciplinaire **HAL**, est destinée au dépôt et à la diffusion de documents scientifiques de niveau recherche, publiés ou non, émanant des établissements d'enseignement et de recherche français ou étrangers, des laboratoires publics ou privés.

Axisymmetric wave propagation in multilayered poroelastic grounds due to a transient acoustic point source

Julien Capeillère^a, Arnaud Mesgouez^{a,*}, Gaëlle Lefeuvre-Mesgouez^a,

^a*Université d'Avignon et des Pays de Vaucluse, UMR EMMAH,
Faculté des Sciences, 33 rue Louis Pasteur, F-84914 Avignon, France*

Abstract

This paper deals with the study of axisymmetric wave propagation in various acoustic / porous stratified media coupling configurations. It presents the theoretical developments of a semi-analytical method, its validation for a limit test-case half-space ground, and an extension to a realistic multilayered seabed, when spherical waves are emitted from a transient point source in water.

Keywords: Stratified poroelastic seabed, Spherical acoustic wave, Axisymmetric geometry, Hankel-Fourier transforms.

1. Introduction

2 The study of wave propagation in seawater-seabed coupling configurations
3 is of interest for underwater acoustics and civil engineering [1, 2, 3]. On
4 the one hand, the acoustic equation models the physical phenomenon in the
5 seawater part, and on the other hand, the Biot equations describe the seabed

*Corresponding author

Email address: arnaud.mesgouez@univ-avignon.fr (Arnaud Mesgouez)

6 part [4, 5]. In such problems, several boundary conditions between the fluid
7 and the top porous layer can be used to model hydraulic exchanges [1, 6, 7].
8 The proposed study focuses on transient wave propagation in a multi-region
9 medium composed of a fluid half-space representing seawater over a stratified
10 poroelastic medium representing the seabed. The source is located within the
11 seawater part and emits spherical transient waves. The purpose is to provide
12 a semi-analytical approach to solve this coupled problem in an axisymmetric
13 configuration.

14 Configurations are often restricted to 2D Cartesian geometries. Three-
15 dimensional Green's function in axisymmetric configurations was first devel-
16 oped by [8] for an acoustic point source located near a half-space poroelastic
17 seabed. Nevertheless, the study was restricted to half-space situations.

18 Focusing on the stratified aspect of the problem, the strategies usually
19 adopted are based on transfer matrix, stiffness matrix or transmission and
20 reflexion matrix methods. The main difficulty deals with the conditioning
21 of matrices, that can be overcome using specific techniques [9]. These meth-
22 ods historically developed for electromagnetic and then viscoelastic problems
23 have been extended to poroelastic media. These developments have been pro-
24 posed for 2D Cartesian geometries with a free surface [9, 10] and then with a
25 coupling with a seawater interaction [11]. In the present article, we propose
26 to extend the previous work to an axisymmetric geometry and to couple the
27 stratified poroelastic medium to a fluid one. Thus, this work can be used
28 as benchmark solutions for numerical approaches, or for comparisons with
29 experimental results. Moreover it represents the first step of the Boundary
30 Element Method. The axisymmetric approach is based on Hankel-Fourier

31 transforms, providing thus an analytical matrix system for the fluid pressure
32 / stresses / displacements / velocities in the frequency-wavenumber domain.
33 To obtain results in the time and space domain, integrations are then per-
34 formed numerically.

35 The paper is organized as follows. Section 2 describes the geometry under
36 study, and proposes analytical solutions to the acoustic equation and Biot
37 equations in the context of multilayered medium and axisymmetric geometry.
38 Section 3 presents a test case to validate the results by a comparison with
39 those of [8], and illustrates both the stratified aspect of the ground and the
40 interface with the seawater.

41 **2. Model formulation**

42 *2.1. Geometry under study*

43 The configuration under investigation is a fluid half-space Ω_0 over a stack
44 of homogeneous and isotropic poroelastic layers Ω_n ($n = 1, \dots, N$), as shown
45 in Fig. 1. The z geometrical axis points upward. The N plane and parallel
46 interfaces are located at $z_n \leq 0$, with $z_0 = 0$. An acoustic point source
47 O_s ($r_s = 0$; $z_s > 0$) in the fluid emits transient spherical waves.

48 *2.2. Multilayered porous medium*

The poroelastic media are modeled using the Biot theory [1, 4, 5]. For
homogeneous and isotropic layers, the physical parameters do not depend
on the spatial coordinates and can be listed as follows: for the saturating
fluid, dynamic viscosity η and density ρ_f ; for the elastic skeleton, density ρ_s
and shear modulus μ as well as connected porosity ϕ , tortuosity a , absolute

permeability κ , Lamé coefficient of the dry matrix λ , and two Biot coefficients β and m . Based on the constitutive equations and the conservation of momentum in porous media, one obtains

$$\left\{ \begin{array}{l} \sigma = (\lambda \nabla \cdot \mathbf{u} - \beta p) \mathbf{I} + 2 \mu \varepsilon, \\ p = -m (\beta \nabla \cdot \mathbf{u} + \nabla \cdot \mathbf{w}), \\ \nabla \sigma = \rho \ddot{\mathbf{u}} + \rho_f \ddot{\mathbf{w}}, \\ -\nabla p = \rho_f \ddot{\mathbf{u}} + \frac{a \rho_f}{\phi} \ddot{\mathbf{w}} + \frac{\eta}{\kappa} \Upsilon * \dot{\mathbf{w}}, \end{array} \right. \quad \begin{array}{l} (1a) \\ (1b) \\ (1c) \\ (1d) \end{array}$$

where \mathbf{u} , \mathbf{U} and $\mathbf{w} = \phi (\mathbf{U} - \mathbf{u})$ are the solid displacement, the fluid displacement and the relative displacement vectors, respectively. \mathbf{I} is the identity tensor, σ is the stress tensor, $\varepsilon = 1/2 (\nabla \mathbf{u} + \nabla^t \mathbf{u})$ is the strain tensor, and p is the pore pressure. $\rho = \phi \rho_f + (1 - \phi) \rho_s$ is the total density. The overlying dot denotes the derivative in terms of time t . $*$ stands for a convolution product in time. The quantity $\frac{\eta}{\kappa} \Upsilon * \dot{\mathbf{w}}$ corresponds to the time domain drag force between the porous skeleton and the pore fluid [12, 13]. Expression for $\Upsilon * \dot{\mathbf{w}}$ depends on the frequency range involved. In the low-frequency range, the relative motion between the fluid and the porous skeleton is of Poiseuille type, and then the expression is given by

$$\Upsilon(t) = \delta(t) \Leftrightarrow \Upsilon(t) * \dot{\mathbf{w}}(t) = \dot{\mathbf{w}}(t)$$

In the high-frequency range, the relative motion between the fluid and the porous skeleton is dominated by the inertial effects. We adopt here the well-known model proposed by [14] and written in the frequency domain. The expression in the time domain is given in [13, 15] with the following form for

the convolution product

$$\Upsilon(t) * \dot{\mathbf{w}}(t) = \frac{1}{\sqrt{\Omega}}(D + \Omega)^{1/2} \dot{\mathbf{w}}(t)$$

49 where $\Omega = \frac{\omega_{\text{JKD}}}{\chi}$ with $\omega_{\text{JKD}} = \frac{\eta\phi}{a\kappa\rho_f}$ the transition radial frequency between
 50 the low- and high-frequency ranges. χ is the Pride number. The operator
 51 $(D + \Omega)^{1/2}$ is a shifted order 1/2 fractional derivative. Note that the drag
 52 force depends on the entire history of $\dot{\mathbf{w}}(t)$.

Pressure and stress components are eliminated from Eqs. (1a)-(1b) and substituted in Eqs. (1c)-(1d), giving a (\mathbf{u}, \mathbf{w}) second-order wave formulation [9, 10]. By introducing the Helmholtz potentials for the solid $(\varphi, \mathbf{\Psi})$ and relative $(\varphi^r, \mathbf{\Psi}^r)$ displacements, the wave formulation yields a system of partial differential equations associated to these potentials as follows

$$\left\{ \begin{array}{l} -\mu \left(\Delta \psi_\theta - \frac{\psi_\theta}{r^2} \right) + ((1 - \phi)\rho_s + \phi\rho_f) \ddot{\psi}_\theta + \rho_f \ddot{\psi}_\theta^r = 0, \quad (2a) \\ \rho_f \ddot{\psi}_\theta + \frac{a\rho_f}{\phi} \ddot{\psi}_\theta^r + \frac{\eta}{\kappa} \frac{1}{\sqrt{\Omega}} (D + \Omega)^{1/2} \dot{\psi}_\theta^r = 0, \quad (2b) \\ (\lambda + 2\mu + m\beta^2) \Delta \varphi + m\beta \Delta \varphi^r - \rho \ddot{\varphi} - \rho_f \ddot{\varphi}^r = 0, \quad (2c) \\ m\beta \Delta \varphi + m \Delta \varphi^r - \rho_f \ddot{\varphi} - \frac{a\rho_f}{\phi} \ddot{\varphi}^r - \frac{\eta}{\kappa} \frac{1}{\sqrt{\Omega}} (D + \Omega)^{1/2} \dot{\varphi}^r = 0. \quad (2d) \end{array} \right.$$

53 Note that when projecting in the axisymmetric geometry, only the θ coordi-
 54 nate is useful for the vector potentials: $\mathbf{\Psi} = \psi_\theta(r, z, t) \mathbf{e}_\theta$.

55 For an axisymmetric configuration, it is relevant to introduce the n th or-
 56 der Hankel (or Fourier-Bessel) transform over the r variable, and the Fourier
 57 transform over the t variable, of an integrable function f , defined as follows
 58 [16]

$$\tilde{f}_n(\xi) = \int_0^{+\infty} r f(r) J_n(\xi r) dr \quad \text{and} \quad f^*(\omega) = \frac{1}{2\pi} \int_{-\infty}^{+\infty} f(t) e^{+i\omega t} dt, \quad (3)$$

59 where ξ is the transform Hankel parameter, ω the radial frequency and J_n
60 the n th order Bessel function of the first kind.

61 In the following, we perform a Fourier transform in time of Eqs. (2a)-(2b)-
62 (2c)-(2d). Then, 0th- and 1st-order Hankel transforms are applied to the
63 scalar and vector potentials, respectively. From equation (2b), a proportion-
64 ality relation between $\widetilde{\psi}_{\theta 1}^{r*}(\xi, z, \omega)$ and $\widetilde{\psi}_{\theta 1}^*(\xi, z, \omega)$ is obtained

$$\widetilde{\psi}_{\theta 1}^{r*}(\xi, z, \omega) = -\frac{\rho_f \omega}{\frac{a \rho_f \omega}{\phi} + i \frac{\eta}{\kappa} \Upsilon^*(\omega)} \widetilde{\psi}_{\theta 1}^*(\xi, z, \omega) = G^*(\omega) \widetilde{\psi}_{\theta 1}^*(\xi, z, \omega). \quad (4)$$

65 Then, the introduction of the above relation in the doubly transformed do-
66 main formulation of Eq. (2a) provides the partial differential equation rela-
67 tive to the S shear wave

$$\frac{\partial^2 \widetilde{\psi}_{\theta 1}^*}{\partial z^2}(\xi, z, \omega) + \left(\frac{\omega^2}{\mu} ((1 - \phi) \rho_s + (\phi + G^*(\omega) \rho_f)) - \xi^2 \right) \widetilde{\psi}_{\theta 1}^*(\xi, z, \omega) = 0. \quad (5)$$

68 Similarly, relative and absolute scalar potentials are linked by

$$\widetilde{\varphi}_{0j}^{r*}(\xi, \omega) = \frac{\rho_f \omega^2 - m \beta (k_{P_j}^2 + \xi^2)}{m (k_{P_j}^2 + \xi^2) - \frac{a \rho_f \omega^2}{\phi} - i \frac{\eta \omega}{\kappa} \Upsilon^*(\omega)} \widetilde{\varphi}_{0j}^*(\xi, \omega) = \widetilde{F}_j^*(\xi, \omega) \widetilde{\varphi}_{0j}^*(\xi, \omega), \quad (6)$$

69 where $j = 1, 2$. The formulation of Eqs. (2c) and (2d) in the doubly trans-
70 formed domain results in two coupled partial differential equations relative
71 to the P_1 and P_2 compressional waves, defined as

$$\left[\left(\frac{\partial^2}{\partial z^2} - \xi^2 \right) \mathbf{K}_P + \omega^2 \mathbf{M} + i \omega \mathbf{C} \right] \widetilde{\Phi}_0^* = \mathbf{0}, \quad (7)$$

72 where $\widetilde{\Phi}_0^* = \left\{ \begin{array}{l} \widetilde{\varphi}_0^*(\xi, z, \omega) \\ \widetilde{\varphi}_0^{r*}(\xi, z, \omega) \end{array} \right\}$, stiffness, mass and damping matrices being

73 respectively

$$\mathbf{K}_P = \begin{bmatrix} \lambda + 2\mu + m\beta^2 & m\beta \\ m\beta & m \end{bmatrix}, \mathbf{M} = \begin{bmatrix} \rho & \rho_f \\ \rho_f & \frac{a\rho_f}{\phi} \end{bmatrix}, \mathbf{C} = \begin{bmatrix} 0 & 0 \\ 0 & \frac{\eta}{\kappa}\Upsilon^*(\omega) \end{bmatrix}. \quad (8)$$

74 From Eqs. (5) and (7), we introduce global wavenumbers k_s and k_{Pj} by the
 75 relations $k_s^2 = k_{zS}^2 + \xi^2 = \frac{\omega^2}{\mu} ((1 - \phi)\rho_s + (\phi + G^*(\omega)\rho_f))$ and $k_{Pj}^2 = k_{zPj}^2 +$
 76 ξ^2 . k_{zS} , k_{zPj} and ξ are the associated vertical wavenumbers and the radial
 77 wavenumber, respectively. Applying the Fourier transform over the z variable
 78 defined as follows

$$\bar{f}(k_z) = \frac{1}{2\pi} \int_{-\infty}^{+\infty} f(z) e^{-ik_z z} dz \quad (9)$$

79 to system (7), yields the dispersion relation when the determinant of matrix is
 80 equal to zero. Then, the general solution relative to the solid phase Helmholtz
 81 potentials of system (5)-(7) can be written as

$$\widetilde{\psi}_{\theta_1}^*(\xi, z, \omega) = \widetilde{\psi}_{\theta_1}^{*I}(\xi, \omega) e^{-ik_{zS}z} + \widetilde{\psi}_{\theta_1}^{*R}(\xi, \omega) e^{ik_{zS}z}, \quad (10)$$

82

$$\begin{aligned} \widetilde{\varphi}_0^*(\xi, z, \omega) &= \widetilde{\varphi}_{01}^{*I}(\xi, \omega) e^{-ik_{zP1}z} + \widetilde{\varphi}_{01}^{*R}(\xi, \omega) e^{ik_{zP1}z} \\ &+ \widetilde{\varphi}_{02}^{*I}(\xi, \omega) e^{-ik_{zP2}z} + \widetilde{\varphi}_{02}^{*R}(\xi, \omega) e^{ik_{zP2}z}, \end{aligned} \quad (11)$$

83 where I and R state the ‘incident’ (or downward) and the ‘reflected’ (or
 84 upward) waves, respectively.

85 The choice of an upward (z) axis, implies that the conditions $\Im m\{k_{zS}\} \geq 0$
 86 as well as $\Im m\{k_{zPj}\} \geq 0$ ($j = 1, 2$) should be satisfied to have a bounded
 87 field far away from the ground surface ($z \rightarrow -\infty$).

88 Besides, for an axisymmetric geometry

$$\widetilde{u}_{r1}^*(\xi, z, \omega) = -\xi \widetilde{\varphi}_0^*(\xi, z, \omega) - \frac{\partial \widetilde{\psi}_{\theta_1}^*}{\partial z}(\xi, z, \omega), \quad (12)$$

$$\tilde{u}_{z_0}^*(\xi, z, \omega) = \frac{\partial \tilde{\varphi}_0^*}{\partial z}(\xi, z, \omega) + \xi \tilde{\psi}_{\theta_1}^*(\xi, z, \omega). \quad (13)$$

Obviously, analogous expressions are obtained for the radial and vertical relative displacement components of vector \mathbf{w} by substituting Helmholtz potentials for the solid displacement by relative ones.

Then, the expressions of $\tilde{u}_{r_1}^*$ and $\tilde{u}_{z_0}^*$ as functions of the scalar ‘incident’ and ‘reflected’ Helmholtz potentials, are obtained from Eqs. (10)-(11) substituted in Eqs. (12)-(13). The same developments are performed for $\tilde{w}_{r_1}^*$ and $\tilde{w}_{z_0}^*$ with relative Helmholtz potentials. In the present axisymmetric configuration, the exact stiffness matrix approach is based on vectors of transformed displacement and stress components [9, 10], defined as

$$\tilde{\mathbf{u}}^* = (\tilde{u}_{r_1}^*, i\tilde{u}_{z_0}^*, i\tilde{w}_{z_0}^*)^t, \quad \tilde{\Sigma}^* = (\tilde{\sigma}_{rz_1}^*, i\tilde{\sigma}_{zz_0}^*, -i\tilde{p}_0^*)^t.$$

90 By using matrix notations, after setting $\tilde{\Phi}^{*I/R} = (\tilde{\varphi}_{01}^{*I/R}, \tilde{\varphi}_{02}^{*I/R}, \tilde{\psi}_{\theta_1}^{*I/R})^t$, one
91 can deduce

$$\begin{Bmatrix} \tilde{\mathbf{u}}^*(\xi, z_{n-1}, \omega) \\ \tilde{\mathbf{u}}^*(\xi, z_n, \omega) \end{Bmatrix} = \begin{bmatrix} \text{Mat}^I & \text{Mat}^{RZ} \\ \text{Mat}^{IZ} & \text{Mat}^R \end{bmatrix} \begin{Bmatrix} \tilde{\Phi}'^{*I}(\xi, \omega) \\ \tilde{\Phi}'^{*R}(\xi, \omega) \end{Bmatrix}, \quad (14)$$

92 where $\tilde{\Phi}'^{*I/R}$ are modified potentials to have a better conditioning of Eq.

93 (14) [9]. $\text{Mat}^{I/R} = \begin{bmatrix} \text{mat}_{pq}^{I/R} \end{bmatrix}$; $p = 1, 2, 3$; $q = 1, 2, 3$ with

$$\begin{cases} \text{mat}_{11}^{I/R} = \text{mat}_{12}^{I/R} = -\xi; & \text{mat}_{13}^I = -\text{mat}_{13}^R = +ik_{zS}; \\ \text{mat}_{21}^I = -\text{mat}_{21}^R = +k_{zP_1}; & \text{mat}_{22}^I = -\text{mat}_{22}^R = +k_{zP_2}; \\ \text{mat}_{23}^{I/R} = +i\xi; & \text{mat}_{31}^I = -\text{mat}_{31}^R = +k_{zP_1}\tilde{F}_1^*(\xi, \omega); \\ \text{mat}_{32}^I = -\text{mat}_{32}^R = +k_{zP_2}\tilde{F}_2^*(\xi, \omega); & \text{mat}_{33}^{I/R} = +i\xi G^*(\omega). \end{cases}$$

94
95
96

97 $Z = \text{Diag}[e^{ik_z P_1 h_n}, e^{ik_z P_2 h_n}, e^{ik_z S h_n}]$ where Diag represents the terms of a diag-
 98 onal matrix. $h_n = z_{n-1} - z_n > 0$ is the height of a specific layer “ n ” bordered
 99 by the upper and the lower depth coordinates, z_{n-1} and z_n , respectively.

100 Using the Biot behaviour law, stress components can be expressed in
 101 terms of transformed displacements

$$\widetilde{\sigma}_{rz_1}^*(\xi, z, \omega) = \mu \left(\frac{\partial \widetilde{u}_{r_1}^*}{\partial z}(\xi, z, \omega) - \xi \widetilde{u}_{z_0}^*(\xi, z, \omega) \right), \quad (15)$$

102

$$\begin{aligned} \widetilde{\sigma}_{zz_0}^*(\xi, z, \omega) &= (\lambda + m\beta^2) \xi \widetilde{u}_{r_1}^*(\xi, z, \omega) + (\lambda + 2\mu + m\beta^2) \frac{\partial \widetilde{u}_{z_0}^*}{\partial z}(\xi, z, \omega) \\ &+ m\beta \xi \widetilde{w}_{r_1}^*(\xi, z, \omega) + m\beta \frac{\partial \widetilde{w}_{z_0}^*}{\partial z}(\xi, z, \omega). \end{aligned} \quad (16)$$

103 Besides, regarding the pore pressure, the equivalent of Eq. (1b) in the doubly
 104 transformed domain is

$$\begin{aligned} \widetilde{p}_0^*(\xi, z, \omega) &= -m \left\{ \beta \left[\xi \widetilde{u}_{r_1}^*(\xi, z, \omega) + \frac{\partial \widetilde{u}_{z_0}^*}{\partial z}(\xi, z, \omega) \right] \right. \\ &\quad \left. + \xi \widetilde{w}_{r_1}^*(\xi, z, \omega) + \frac{\partial \widetilde{w}_{z_0}^*}{\partial z}(\xi, z, \omega) \right\}. \end{aligned} \quad (17)$$

105 Then, the relation between stresses and Helmholtz potentials is given by

$$\begin{Bmatrix} \widetilde{\Sigma}^*(\xi, z_{n-1}, \omega) \\ -\widetilde{\Sigma}^*(\xi, z_n, \omega) \end{Bmatrix} = \begin{bmatrix} S^I & S^{RZ} \\ -S^IZ & -S^R \end{bmatrix} \begin{Bmatrix} \widetilde{\Phi}'^{*I}(\xi, \omega) \\ \widetilde{\Phi}'^{*R}(\xi, \omega) \end{Bmatrix}, \quad (18)$$

106 where $S^{I/R} = \begin{bmatrix} S^{I/R} \\ s_{pq} \end{bmatrix}$; $p = 1, 2, 3$; $q = 1, 2, 3$ with

107

$$\begin{cases}
s_{11}^I = -s_{11}^R = +2i\mu\xi k_{zP_1}; & s_{12}^I = -s_{12}^R = +2i\mu\xi k_{zP_2}; \\
s_{13}^{I/R} = +\mu(k_{zS}^2 - \xi^2); & s_{21}^I = s_{21}^R = -i[(k_{zP_1}^2 + \xi^2)(\lambda + \\
& m\beta^2 + m\beta\widetilde{F}_1^*(\xi, \omega)) + 2\mu k_{zP_1}^2]; \\
s_{22}^I = s_{22}^R = -i[(k_{zP_2}^2 + \xi^2)(\lambda + \\
& m\beta^2 + m\beta\widetilde{F}_2^*(\xi, \omega)) + 2\mu k_{zP_2}^2]; & s_{23}^I = -s_{23}^R = +2\mu\xi k_{zS}; \\
s_{31}^{I/R} = -im(k_{zP_1}^2 + \xi^2)(\widetilde{F}_1^*(\xi, \omega) + \beta); \\
s_{32}^{I/R} = -im(k_{zP_2}^2 + \xi^2)(\widetilde{F}_2^*(\xi, \omega) + \beta); & s_{33}^{I/R} = 0.
\end{cases}$$

Finally, analytical expressions for transformed displacement vectors are written in condensed form as

$$[\mathbf{T}_{\text{layer}_n}]_{6 \times 6} \begin{Bmatrix} \widetilde{\mathbf{u}}^*(\xi, z_{n-1}, \omega) \\ \widetilde{\mathbf{u}}^*(\xi, z_n, \omega) \end{Bmatrix} = \begin{Bmatrix} \widetilde{\Sigma}^*(\xi, z_{n-1}, \omega) \\ -\widetilde{\Sigma}^*(\xi, z_n, \omega) \end{Bmatrix}. \quad (19)$$

A conventional assembling technique between the layers is then performed [17, 18]. As $[\mathbf{T}_{\text{layer}_n}]$ is a 6×6 matrix, the global resulting matrix system has dimension $3(N+1) \times 3(N+1)$.

2.3. Acoustic medium

This part presents the analytical model formulation of wave propagation coming from an acoustic point source applied at O_s (Fig. 1), in the water semi-infinite domain Ω_0 , characterized by celerity of waves c and by density ρ_f , assumed to be the same as in the porous media Ω_n .

The acoustic equations are written as follows

$$\begin{cases} \ddot{\mathbf{U}}(r, z, t) = -\frac{1}{\rho_f} \nabla p(r, z, t), & (20a) \\ \Delta p(r, z, t) - \frac{1}{c^2} \ddot{p}(r, z, t) = -s(r, z, t) = -S(t) \delta(r - r_s) \delta(z - z_s) & (20b) \end{cases}$$

120 where p is the acoustic pressure, \mathbf{U} is the fluid displacement and $s(r, z, t)$ is
 121 the impulse transient superpressure emitted from point O_s . $S(t)$ is a causal
 122 source term and δ is the Dirac function.

123 In the following, we introduce the fluid global wavenumber k_f , linked to its
 124 vertical (k_{zf}) and radial (ξ) components by $k_f^2 = k_{zf}^2 + \xi^2 = \frac{\omega^2}{c^2}$, and use the
 125 mathematical property

$$\tilde{\delta}_0(\xi) = \int_0^{+\infty} r \delta(r) J_0(\xi r) dr = \frac{1}{2\pi}. \quad (21)$$

126 Then, the partial differential equation relative to the pressure wave is ob-
 127 tained from the formulation of Eq. (20b) in the Fourier and 0th-order Hankel
 128 transform domain, as

$$\frac{\partial^2 \tilde{p}_0^*}{\partial z^2}(\xi, z, \omega) + k_{zf}^2 \tilde{p}_0^*(\xi, z, \omega) = -\frac{S^*(\omega)}{2\pi} \delta(z - z_s). \quad (22)$$

129 The solution to the above inhomogeneous equation results in the summation
 130 of two components:

- 131 - the complementary part $\tilde{p}_{C0}^*(\xi, z, \omega)$ corresponding to the solution of the
- 132 homogeneous equation associated to Eq. (22),
- 133 - the principal part $\tilde{p}_{P0}^*(\xi, z, \omega)$ which is a specific solution of Eq. (22).

134 On the one hand, the complementary part of the solution is given by

$$\tilde{p}_{C0}^*(\xi, z, \omega) = \tilde{\mathcal{P}}^*(\xi, \omega) e^{ik_{zf}z} + \tilde{\mathcal{Q}}^*(\xi, \omega) e^{-ik_{zf}z}, \quad (23)$$

135 $\tilde{\mathcal{P}}^*(\xi, \omega)$ and $\tilde{\mathcal{Q}}^*(\xi, \omega)$ being the amplitudes, $\tilde{\mathcal{Q}}^*(\xi, \omega) = 0$ and $\Im m(k_{zf}) \geq 0$
 136 to satisfy the convergence condition when $z \rightarrow +\infty$.

137 On the other hand, the calculation of the principal part of the solution is
 138 inspired by [19, 20]. Concisely, the key steps are:

139 (i) Setting the principal part of the solution as a simple Fourier integral
 140 expression

$$\widetilde{p}_{P_0}^*(\xi, z, \omega) = \int_{-\infty}^{+\infty} \mathcal{A}(\kappa_z) e^{i\kappa_z z} d\kappa_z. \quad (24)$$

141 (ii) Searching function $\mathcal{A}(\kappa_z)$ by introducing Eq. (24) in Eq. (22), multi-
 142 plying the obtained equation by $e^{-i\kappa_z z}$ (where $\kappa_z \in \mathbb{R}$), integrating over the
 143 z variable from $-\infty$ to $+\infty$, and using some mathematical properties of the
 144 Dirac function to obtain

$$\mathcal{A}(\kappa_z) = -\frac{S^*(\omega)}{(2\pi)^2} \frac{e^{-i\kappa_z z_s}}{k_{zf}^2 - \kappa_z^2}. \quad (25)$$

145 (iii) Rewriting the principal part of the solution gives

$$\widetilde{p}_{P_0}^*(\xi, z, \omega) = \frac{S^*(\omega)}{(2\pi)^2} I(z - z_s, k_{zf}), \quad (26)$$

146 where [19]

$$I(z - z_s, k_{zf}) = \int_{-\infty}^{+\infty} \frac{e^{i\kappa_z(z-z_s)}}{k_{zf}^2 - \kappa_z^2} d\kappa_z = \pm i\pi \frac{e^{i\pm k_{zf}|z-z_s|}}{k_{zf}}. \quad (27)$$

147 (iv) Finally obtaining the single physically valid solution, satisfying the Som-
 148 merfeld condition [20]

149

$$\widetilde{p}_{P_0}^*(\xi, z, \omega) = \frac{iS^*(\omega)}{4\pi} \frac{e^{ik_{zf}|z-z_s|}}{k_{zf}}. \quad (28)$$

150 Solution (28) corresponds to the one obtained in [8, 20]. Indeed, these authors
 151 provide a Green's function as a solution of a cylindrical Helmholtz equation,
 152 which corresponds to the Fourier transform in time of Eq. (20b). Then, they
 153 calculate $\widetilde{p}_{P_0}^*(\xi, z, \omega)$ by using a Sommerfeld integral decomposition of the
 154 simply transformed domain solution.

155 *2.4. Interface equations*

156 The geometry under study leads to a set of interface equations along the
 157 N plane interfaces z_n ($n = 0, \dots, N - 1$). For this purpose, we denote $[g]_n$
 158 the jump in a function g from Ω_n to Ω_{n+1} across z_n as

$$\begin{aligned} [g]_n &= \lim_{\varepsilon \rightarrow 0, \varepsilon > 0} g(r, z_n + \varepsilon, t) - \lim_{\varepsilon \rightarrow 0, \varepsilon > 0} g(r, z_n - \varepsilon, t) \\ &= (g)_n^+ - (g)_n^- \end{aligned} \quad (29)$$

159 - The porous / porous interfaces z_n ($n = 1, \dots, N - 1$) are assumed to be in
 160 perfect bonded contact [1]

$$\begin{aligned} [u_r(r, z, t)]_n &= 0, & [u_z(r, z, t)]_n &= 0, & [w_z(r, z, t)]_n &= 0, \\ [\sigma_{rz}(r, z, t)]_n &= 0, & [\sigma_{zz}(r, z, t)]_n &= 0, & [p(r, z, t)]_n &= 0. \end{aligned} \quad (30)$$

- The fluid / porous interface $z_0 = 0$ is modeled with the following interface conditions [1, 6, 7]

$$\begin{cases} (u_z(r, z, t))_0^- + (w_z(r, z, t))_0^- = (U_z(r, z, t))_0^+, & (31a) \\ (\sigma_{rz}(r, z, t))_0^- = 0, & (31b) \\ (\sigma_{zz}(r, z, t))_0^- = -(p(r, z, t))_0^+, & (31c) \\ -[p(r, z, t)]_0 = \frac{1}{\mathcal{K}} (\dot{w}_z(r, z, t))_0^-. & (31d) \end{cases}$$

161 where \mathcal{K} is the hydraulic permeability of the interface. The case $\mathcal{K} \rightarrow +\infty$
 162 describes *open pores*. For $\mathcal{K} \rightarrow 0$, Eq. (31d) is replaced by $(\dot{w}_z(r, z, t))_0^- =$
 163 0 , stating *sealed pores*. An intermediate state for $\mathcal{K} \in]0; +\infty[$ describes
 164 *imperfect pores*.

165 The formulation of the fluid /porous interface equations (31a)-(31c)-(31d)
 166 in the doubly transformed domain enables both to determine the amplitude

167 $\tilde{\mathcal{P}}^*(\xi, \omega)$ of the ‘reflected’ pressure wave in the fluid, and as a result to provide
 168 the following matrix block

$$\begin{aligned}
 & \begin{bmatrix} -\frac{i\rho_f\omega^2}{k_{zf}} & -\frac{i\rho_f\omega^2}{k_{zf}} \\ -\frac{i\rho_f\omega^2}{k_{zf}} & -\frac{i\rho_f\omega^2}{k_{zf}} - \frac{i\omega}{\mathcal{K}} \end{bmatrix} \begin{Bmatrix} i(\tilde{u}_{z0}^*(\xi, z, \omega))_0^- \\ i(\tilde{w}_{z0}^*(\xi, z, \omega))_0^- \end{Bmatrix} \\
 = & \begin{Bmatrix} -i(\tilde{\sigma}_{zz0}^*(\xi, z, \omega))_0^- + \frac{S^*(\omega)}{2\pi} \frac{e^{ik_{zf}z_s}}{k_{zf}} \\ i(\tilde{p}_0^*(\xi, z, \omega))_0^- + \frac{S^*(\omega)}{2\pi} \frac{e^{ik_{zf}z_s}}{k_{zf}} \end{Bmatrix}. \quad (32)
 \end{aligned}$$

169 Eq. (32) is assembled to Eq. (19) to give the radial and vertical solid and
 170 relative displacements at each interface. The transformed displacements,
 171 stresses, velocities and acoustic pressure everywhere inside each domain Ω_n
 172 can then be obtained analytically. The latter quantities are subsequently
 173 calculated in the spatio-temporal domain by means of inverse Hankel-Fourier
 174 transforms. For example, the acoustic or pore pressure can be written as
 175 follows

$$p(r, z, t) = \int_0^{+\infty} 2 \Re e \left(\left\{ \int_0^{+\infty} \xi \tilde{p}_0^*(\xi, z, \omega) J_0(\xi r) d\xi \right\} e^{-i\omega t} \right) d\omega \quad (33)$$

176 The integral over the radial wavenumber, which presents an oscillatory be-
 177 havior due to factor $J_0(\xi r)$ and for which the envelope of the maximum am-
 178 plitudes shows sharp peaks, is performed using an adaptive Filon quadrature,
 179 [21, 22]. The adaptive procedure consists in dividing the entire interval into
 180 several parts based on what is known about $\tilde{p}_0^*(\xi, z, \omega)$. Because of the sharp
 181 changes in the integrand occurring around the wavenumbers of the propagat-
 182 ing waves, the wavenumbers are calculated and sorted out. The quadrature
 183 is performed by discretizing finely in their neighborhood and more coarsely

184 farther away. The integral is truncated depending on the highest wavenum-
 185 ber and adapted to each frequency. As for the numerical processing over ω ,
 186 the quadrature is done using a Simpson scheme. Numerical values used for
 187 the various discretizations are those of [11].

188 3. Results and discussion

189 In this section, we propose firstly to validate the above theoretical for-
 190 mulation by using a half-space porous medium such as in [8]. To do that,
 191 we consider a limit test-case of the stratified configuration, composed of two
 192 layers presenting the same physical properties. Once the semi-analytical ap-
 193 proach validated, we present new results coming from a seabed [23, 24] made
 194 of ten layers presenting various properties, as an extension of the half-space
 195 porous ground.

196 3.1. Half-space test-case configuration

Porous and fluid parameters are [8]: $\lambda = 10.0 \times 10^9$ Pa, $\mu = 5.0 \times$
 10^9 Pa, $\rho_s = 2.5 \times 10^3$ kg.m⁻³, $\rho_f = 1.0 \times 10^3$ kg.m⁻³, $a = 3$, $\beta = 0.7$,
 $m = 10.0 \times 10^9$ Pa, $\phi = 0.33$, $\eta = 1.0 \times 10^{-3}$ Pa.s, $\kappa = 10^{-8}$ m² as well as,

$$\Upsilon^*(\omega) = \left(1 + i\frac{\omega}{\Omega}\right)^{1/2}, \quad \Omega = \frac{\eta \phi}{a \kappa \rho_f \chi} \text{ with } \chi = 0.5 \text{ [14].}$$

197 In the water domain Ω_0 : $\rho_f = 1.0 \times 10^3$ kg.m⁻³, $c = 1414.0$ m.s⁻¹.

198 The emission point source is located at $z_s = 10$ m and the observation ones
 199 are pointed by $r = 20$ m and $z = \pm 20$ m. Such as in [8], $S(t)$ is a Ricker
 200 wavelet and $S^*(\omega)$ its Fourier transform

$$S(t) = ((1 - 2\hat{\alpha}^2(t - \hat{\beta})^2)e^{-\hat{\alpha}^2(t - \hat{\beta})^2}) \quad \text{and} \quad S^*(\omega) = \frac{\omega^2}{4\hat{\alpha}^3\sqrt{\pi}}e^{(i\hat{\beta}\omega - \frac{\omega^2}{4\hat{\alpha}^2})}, \quad (34)$$

201 where $\hat{\alpha} = \omega_0/2$ and $\hat{\beta} = t_s$, $\omega_0 = 2\pi f_0$ ($f_0 = 1.0 \times 10^3$ Hz) and $t_s = 2.5 \times$
 202 10^{-3} s being, respectively the central angular frequency and a shift in time.

203 As regards time evolution of pore pressure and fluid pressure, Fig. 2 shows
 204 that there is an excellent agreement between the results proposed by [8] and
 205 those obtained from our calculations. Both in permeable and impermeable
 206 cases, it checks the validity of the analytical approach in the half-space limit
 207 test-case.

208 3.2. Extension to a stratified poroelastic seabed

The regarded configuration is built from mechanical data taken from [23,
 24]. It corresponds to a more realistic description of a seabed. To model
 the stratified ground and to illustrate the capabilities of our approach, we
 have chosen a ten layer geometry coupled to a half-space configuration. In
 the porous medium, the unchanged parameters are: $a = 1.25$, $\rho_s = 2.65 \times$
 10^3 kg.m⁻³ as well as the compressibility of the solid skeleton, $\chi_s = 36$ GPa,
 and of the fluid volume, $\chi_f = 2$ GPa. The Lamé constants are linked in this
 study by $\lambda = 2\mu$. Ranges of physical characteristics from the first layer to
 the half-space are: $\phi \in [0.5; 0.2]$, $\kappa \in [10^{-9}; 10^{-12}]$ m² and $\mu \in [10^7; 10^9]$
 Pa. From one stratum to another, only one of these three parameter values
 is modified as indicated in Tab. 1, as well as the related ones. The two Biot
 coefficients β and m are given by

$$\beta = 1 - \frac{\chi_o}{\chi_s}, \quad \frac{1}{m} = \frac{\beta - \phi}{\chi_s} + \frac{\phi}{\chi_f}, \quad \text{where } \chi_o = \lambda + \frac{2}{3}\mu.$$

209 Parameters relative to the nature of the point source and to the water are
 210 the same as for the half-space test-case situation, the only differences are:
 211 $z_s = 5$ m and the observation points are located at $r = 1$ m and $z = \pm 1$ cm

212 or $z = -80$ cm.

213

Layer n	Height h_n (m)	Porosity ϕ	Absolute permeability κ (m^2)	Shear modulus μ (Pa)
$n = 1$	0.1	0.5	1×10^{-9}	1×10^7
$n = 2$	0.1	0.5	1×10^{-9}	5×10^7
$n = 3$	0.4	0.4	1×10^{-9}	5×10^7
$n = 4$	0.4	0.4	5×10^{-10}	5×10^7
$n = 5$	1.0	0.4	5×10^{-10}	1×10^8
$n = 6$	1.0	0.3	5×10^{-10}	1×10^8
$n = 7$	2.0	0.3	1×10^{-11}	1×10^8
$n = 8$	5.0	0.3	1×10^{-11}	5×10^8
$n = 9$	5.0	0.2	1×10^{-11}	5×10^8
$n = 10$	10.0	0.2	1×10^{-11}	1×10^9
Half-space	$+\infty$	0.2	1×10^{-12}	1×10^9

Table 1: Height of each layer and parameter values changing from one layer to another in the seabed

Firstly, Fig. 3 shows very similar time evolutions of fluid pressure at $z = 1$ cm observation height, both for sealed, imperfect and open pore interfaces between seawater and seabed. This means that the nature of the contact does not have any influence on the fluid pressure for the configuration under study. Secondly, considering only the impermeable cases, Fig. 3 emphasizes the fact that the properties of the first layer force the fluid

pressure behaviour in the seabed when observation point is very close of the $z_0 = 0$ interface. Thirdly, central arrival time of the acoustic compressional wave is given by

$$t_f = \frac{\sqrt{(z_s - z)^2 + r^2}}{c} + t_s = 6.1 \text{ ms.}$$

214

215 In contrast, Fig. 4 clearly proves that the hydraulic permeability coefficient
 216 value has a strong impact on temporal variation of the vertical displacement
 217 at $z = -1$ cm observation height, in the first layer of the seabed. Note
 218 that this trend is very attenuated when considering stresses in the seabed,
 219 not shown here.

220 Besides the comparison between Fig. 4 and Fig. 5 highlights the multiple
 221 wave reflections at the porous / porous interfaces in the seabed. In addition,
 222 the confrontation between half-space and multilayered results yields higher
 223 differences in the intermediate case than those obtained in the extreme situ-
 224 ations.

225 In the fourth layer, at $z = -80$ cm observation height (Fig. 6), the nature
 226 of the contact does not have influence on the first displacement peaks any
 227 more. This time, the differences due to the kind of hydraulic interface is seen
 228 on the part of the response relative to the reflection waves ($t > 9$ ms).

229 4. Conclusions

230 An axisymmetric model of wave propagation in poroelastic / acoustic
 231 configurations, has been presented, validated and extended by using a semi-
 232 analytical method. The theoretical development has been based on a matrix

233 block assembling technique for the porous layers and the fluid domain and
234 takes into account various interface conditions. A half-space porous ground
235 as a limit test-case of our multilayered medium has been considered to vali-
236 date the analytical model. Indeed, regarding pore and fluid pressures, there
237 is a very good agreement between the results coming from [8] and our calcu-
238 lations, whatever the pore nature. Then, the approach has been applied to
239 a stratified seabed, as an extension of the half-space porous soil, providing
240 new results which emphasize the variations in time of mechanical quantities.

241 From the obtained displacements and stresses, a future investigation con-
242 sists in estimating mechanical and hydrological parameters of the systems
243 under study. In parallel, the results could be compared to those issuing
244 from finite difference, element and/or volume approaches or other analytical
245 formulations such as transfer or transmission and reflexion matrices.

246 [1] T. Bourbié, O. Coussy, B. Zinszner, *Acoustics of Porous Media*, Gulf
247 Publishing Company (1987).

248 [2] F.B. Jensen, W.A. Kuperman, M.B. Porter, H. Schmidt, *Computa-*
249 *tional Ocean Acoustics*, Springer (2011).

250 [3] J.F. Semblat, A. Pecker, *Waves and Vibrations in Soils: Earthquakes,*
251 *Traffic, Shocks, Construction Works*, IUSS Press (2009).

252 [4] M. A. Biot, Theory of propagation of elastic waves in a fluid-saturated
253 porous solid. I: Low-frequency range, *Journal of the Acoustical Society*
254 *of America*, 28-2 (1956), 168-178.

255 [5] J. M. Carcione, *Wave Fields in Real Media: Wave Propagation in*

- 256 Anisotropic, Anelastic, Porous and Electromagnetic Media, Elsevier
257 (2007).
- 258 [6] B. Gurevich, M. Schoenberg, Interface conditions for Biot's equations
259 of poroelasticity, *Journal of the Acoustical Society of America*, 105-5
260 (1999), 2585-2589.
- 261 [7] S. Feng, D. L. Johnson, High-frequency acoustic properties of a fluid /
262 porous solid interface. I. New surface mode, *Journal of the Acoustical*
263 *Society of America*, 74-3 (1983), 906-914.
- 264 [8] J. F. Lu, D. S. Jeng, Green's function for a harmonic acoustic point
265 source within seawater overlying a saturated poroelastic seabed, *Jour-*
266 *nal of Sound and Vibration*, 307 (2007), 172-186.
- 267 [9] A. Mesgouez, G. Lefeuvre-Mesgouez, Transient solution for multilayered
268 poroviscoelastic media obtained by an exact stiffness matrix formula-
269 tion, *International Journal for Numerical and Analytical Methods in*
270 *Geomechanics*, 33 (2009), 1911-1931.
- 271 [10] G. Degrande, G. De Roeck, P. Van Den Broeck, D. M. J. Smeulders,
272 Wave propagation in layered dry, saturated and unsaturated poroelas-
273 tic media, *International Journal of Solids and Structures*, 35 (1998),
274 4753-4778.
- 275 [11] G. Lefeuvre-Mesgouez, A. Mesgouez, G. Chiavassa, B. Lombard, Semi-
276 analytical and numerical methods for computing transient waves in
277 2D acoustic / poroelastic stratified media, *Wave Motion*, 49-7 (2012),
278 667-680.

- 279 [12] J.F. Lu, A. Hanyga, Fundamental solution for a layered porous half
280 space subject to a vertical point force or a point fluid source, *Computational Mechanics*, 35 (2005), 376-391.
281
- 282 [13] E. Blanc, G. Chiavassa, B. Lombard, Biot-JKD model: Simulation of
283 1D transient poroelastic waves with fractional derivatives, *Journal of Computational Physics*, 237 (2013), 1-20.
284
- 285 [14] D. L. Johnson, J. Koplik, R. Dashen, Theory of dynamic permeability and tortuosity in fluid-saturated porous media. *Journal of Fluid Mechanics*, 176 (1987), 379-402.
286
287
- 288 [15] J.F. Lu, A. Hanyga, Wave field simulation for heterogeneous porous
289 media with singular memory drag force, *Journal of Computational Physics*, 208 (2005), 651-674.
290
- 291 [16] M. Abramowitz, I. A. Stegun, *Handbook of Mathematical Functions with Formulas, Graphs, and Mathematical Tables*, 10th ed., National Bureau of Standards Applied Mathematics Series (1972).
292
293
- 294 [17] R.K.N.D. Rajapakse, T. Senjuntichai, Dynamic response of a multi-layered poroelastic medium, *Earthquake Engineering and Structural Dynamics*, 24 (1995), 703-722.
295
296
- 297 [18] D.V. Jones, D. Le Houédec, M. Petyt, Ground vibrations due to a rectangular harmonic load, *Journal of Sound and Vibration*, 212-1 (1998),
298 61-74.
299
- 300 [19] P. M. Morse et H. Feshbach, *Methods of theoretical physics*, Mc Graw Hill, New York (1953).
301

- 302 [20] K. Aki, P. G. Richards, Quantitative Seismology : Theory and Methods
303 I, San Francisco (1980).
- 304 [21] R.Barakat, E. Parshall, Numerical evaluation of the zero-order Han-
305 kel transform using Filon quadrature philosophy, Applied Mathematics
306 Letters, 9-5 (1996), 21-26.
- 307 [22] R.Barakat, B.H. Sandler, Evaluation of the first-order Hankel trans-
308 forms using Filon quadrature philosophy, Applied Mathematics Let-
309 ters, 11-1 (1998), 127-131.
- 310 [23] R. D. Stoll, Reflection of acoustic waves at a water-sediment interface,
311 Journal of the Acoustical Society of America, 70-1 (1981), 149-156.
- 312 [24] N. P. Chotiros, An inversion for Biot parameters in water saturated
313 sand, Journal of the Acoustical Society of America, 112-5 (2002), 1853-
314 1868.

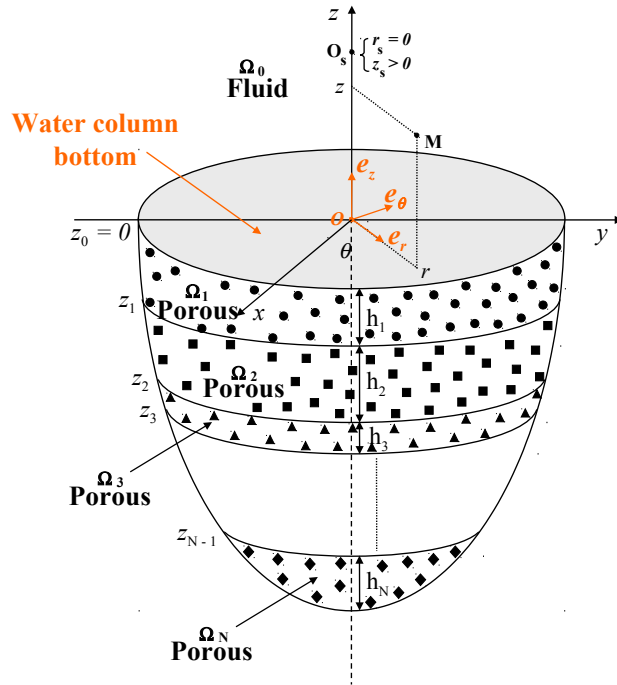
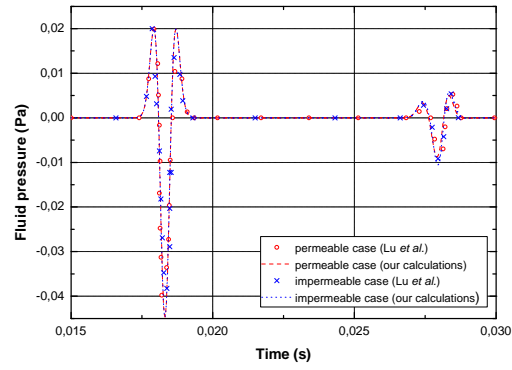
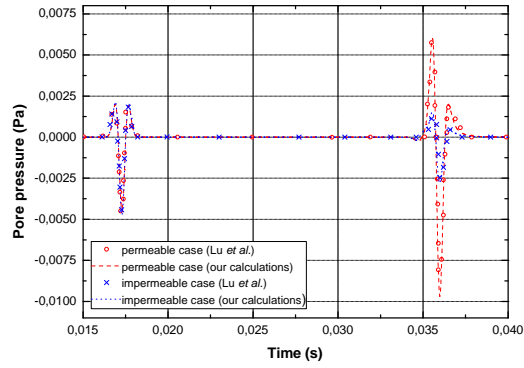


Figure 1: Axisymmetric geometry used for the multilayered poroelastic / acoustic media



(a)



(b)

Figure 2: Time evolution of fluid pressure (up) and pore pressure (down) for permeable and impermeable cases, obtained by [8] and our calculations

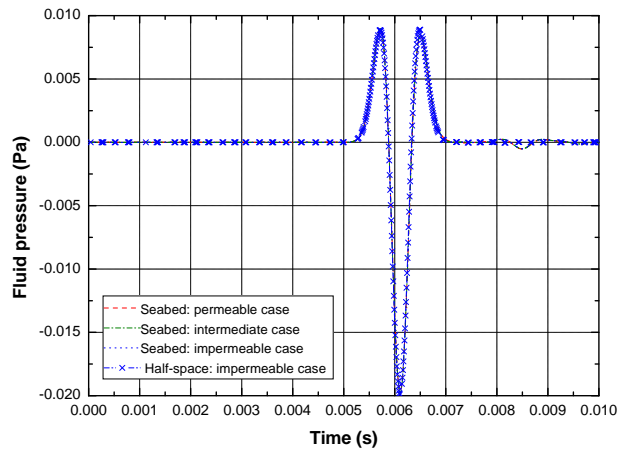


Figure 3: Time evolution of fluid pressure at $z = 1$ cm observation height, for permeable and intermediate ($\mathcal{K} = 5 \times 10^{-10} \text{ m.s}^{-1}.\text{Pa}^{-1}$) cases in the seabed configuration, and for impermeable case in both the seabed and the half-space corresponding situation

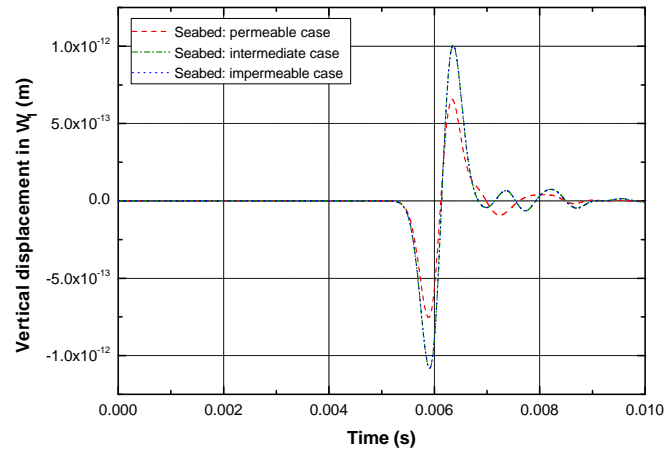


Figure 4: Time evolution of vertical displacement in the first layer at $z = -1$ cm observation height, for permeable, intermediate ($\mathcal{K} = 5 \times 10^{-10} \text{ m.s}^{-1}.\text{Pa}^{-1}$) and impermeable cases in the seabed configuration

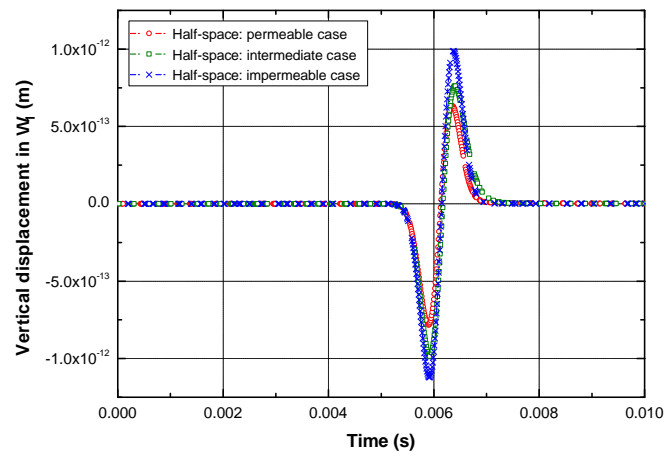


Figure 5: Time evolution of vertical displacement in the half-space corresponding situation to that of Fig. 3

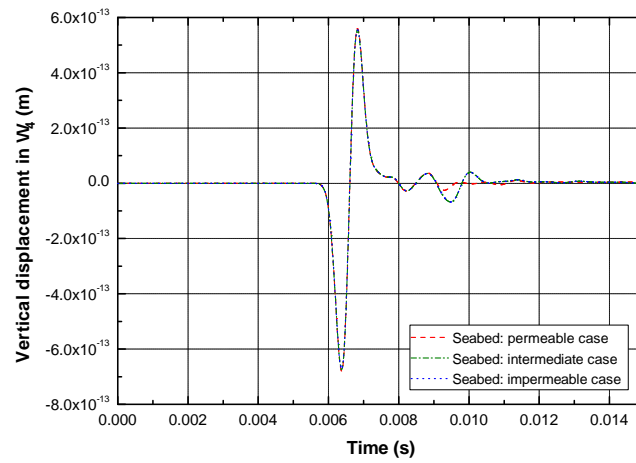


Figure 6: Time evolution of vertical displacement in the fourth layer at $z = -80$ cm observation height, for permeable, intermediate ($\mathcal{K} = 5 \times 10^{-10} \text{ m.s}^{-1}.\text{Pa}^{-1}$) and impermeable cases in the seabed configuration